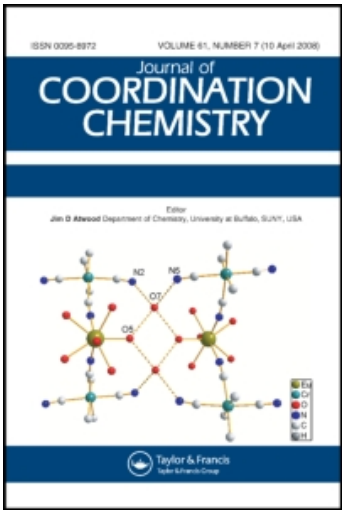

Journal of Coordination Chemistry
Publication details, including instructions for authors and subscription information:
http://www.informaworld.com/smpp/title~content=t713455674

Studies on Cu(II)-mixed ligand complexes containing a sulfa drug and some enzyme constituents

M. Sivasankaran Nair[a]; S. Regupathy[a]
[a] Department of Chemistry, Manonmaniam Sundaranar University, Tirunelveli-627 012, Tamil Nadu, India

First published on: 12 November 2009

To cite this Article Nair, M. Sivasankaran and Regupathy, S.(2010) 'Studies on Cu(II)-mixed ligand complexes containing a sulfa drug and some enzyme constituents', Journal of Coordination Chemistry, 63: 2, 361 — 372, First published on: 12 November 2009 (iFirst)
To link to this Article: DOI: 10.1080/00958970903398069
URL: http://dx.doi.org/10.1080/00958970903398069

Journal of Coordination Chemistry
Vol. 63, No. 2, 20 January 2010, 361–372

Taylor & Francis
Taylor & Francis Group

Studies on Cu(II)-mixed ligand complexes containing a sulfa drug and some enzyme constituents

M. SIVASANKARAN NAIR* and S. REGUPATHY

Department of Chemistry, Manonmaniam Sundaranar University, Tirunelveli – 627 012, Tamil Nadu, India

(*Received 3 March 2009; in final form 12 August 2009*)

Equilibrium studies of Cu(II)-mixed ligand systems involving sulfathiazole (stz) as ligand (A) and enzyme constituents, namely, imidazole (him), benzimidazole (bim), histamine (hist), and histidine (his) as ligand (B) have been investigated by pH metrically at 37°C and $I = 0.15\,\text{mol}\,\text{dm}^{-3}$ ($NaClO_4$). Analysis of the data showed the presence of CuABH, CuAB, and $CuAB_2$ species. The proton in CuABH is attached to B (B = hist/his). In CuAB species, stz binds the metal via the oxygen of $-SO_2NH$ and nitrogen of thiazolidine ring and bim, him, hist, and his(B), respectively, bind in mono-, bi-, and tridentate modes. CuAB in Cu(II)–stz(A)–hist/his(B) systems and $CuAB_2$ in the corresponding him/bim systems were isolated. Magnetic susceptibility data coupled with electronic spectral analysis suggest distorted octahedral geometry for the complexes, supported by the *g* tensor values calculated from ESR spectra. The vibrational spectral data indicate the mode of binding. Thermal behaviors of complexes were studied by TG and DTA. X-ray diffraction data indicate that the complex is microcrystalline. SEM analysis indicates the dislike morphology for $CuAB_2$ in the him system and monoclinic-shaped structure for CuAB. The electrochemical behavior of complexes in MeCN at 298 K shows a quasi-reversible peak and two irreversible peaks. Antimicrobial activity and CT DNA cleavage of the complexes show higher activity for mixed ligand complexes.

Keywords: Sulfathiazole; Stability constants; Spectroscopy; XRD; Microbial activity

1. Introduction

Sulfanilamide and its *N*-substituted compounds are well-known sulfadrugs [1–3]. Metal complexes of sulfadrugs play an important role in metabolic and toxicological function in biological systems [4–7]. Many sulfadrugs show increased biological activity when administered in the form of metal complexes [8–11]. Action of a drug requires specific enzyme as catalyst. Many Cu(II) complexes show increased activity and play specific roles in enzymatic processes [12–14]. However, related studies with salen-type complexes yield useful results [15–17]. To throw more light on the interaction of sulfadrugs with metal ions, a systematic study on the interaction of Cu(II) with sulfathiazole (stz) in the presence of imidazole (him), benzimidazole (bim), histamine (hist), and histidine (his) (figure 1) has been undertaken. Cu(II) complexes of sulfathiazole with him, bim, hist, and his have also been synthesized and characterized

*Corresponding author. Email: msnairchem@rediffmail.com

Journal of Coordination Chemistry
ISSN 0095-8972 print/ISSN 1029-0389 online © 2010 Taylor & Francis
DOI: 10.1080/00958970903398069

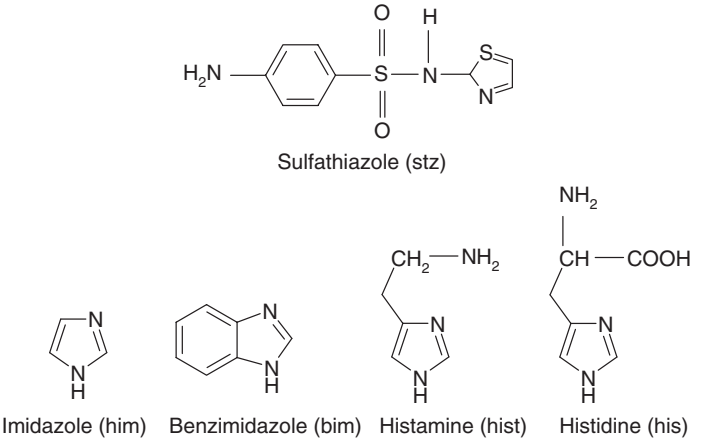

Figure 1. Structure of the ligands.

using analytical, conductance, magnetic susceptibility, electronic and vibrational spectral analysis, ESR studies, TGA and DTA, powder XRD, SEM, and electrochemical studies. The biological activities of the complexes were tested against bacteria *Salmonella typhi*, yeast *Saccharomyces cerevisae*, and fungi *Lapsiodiplodia theobrome* and *Fusarium oxysporum*, using ampicillin in DMF as control. DNA cleavage activities of the complexes were tested against CT DNA using gel electrophoresis in the presence of H_2O_2.

2. Experimental

2.1. *Materials and physical measurements*

All ligands used were extra pure Sigma products. Doubly distilled conductivity water was used for the preparation of all solutions. The pH titrations were carried out at 37°C and $I = 0.15\,\text{mol dm}^{-3}$ ($NaClO_4$) under nitrogen with a digital pH meter (M/s. Systronics 305) with glass and calomel electrode assembly with an accuracy of ± 0.01 of a pH unit [18–20]. Titrations on the mixed ligand complex systems were done on 50 mL portions of solutions containing low concentrations (0.002, 0.0025, and 0.003 M) of $Cu(ClO_4)_2$, stz (A), and ligand (B) in 1 : 1 : 1 and 1 : 1 : 2 ratios with known volumes of standard CO_2-free NaOH. The Cu(II)–stz(A) binary system has been re-investigated under the present experimental conditions and the stability constant data for the Cu(II)–bim, him, hist, and his binary systems were taken from the literature [19, 21] (table 1). The pH titration data were processed using SCOGS computer program [22, 23], and the results are reported in table 2.

2.2. *Preparation of complexes*

The binary complex of stz(A) with Cu(II) was prepared by adding a mixture of 199 mg, (5 m mole) of copper acetate in 20 mL of water and 255 mg (5 m mole) of stz in 20 mL aqueous ethanol. The CuAB complexes in Cu(II)–stz(A)–hist/his(B) were prepared by the mixing 199 mg (5 m mole) of copper acetate in 20 mL of water, 255 mg (5 m mole) of

Table 1. Stability constants for the proton and parent binary complexes of Cu(II) with stz*, him, bim, hist, and his systems at 37°C and $I = 0.15\,\text{mol dm}^{-3}$ ($NaClO_4$).

	Cu(II)–ligand B				
Parameters	stz[a]	him[b]	bim[c]	hist[b]	his[b]
$\log \beta_{HB}$	7.17(3)	6.95	5.68	9.39	8.96
$\log \beta_{H_2B}$	9.23(8)	–	–	15.34	14.96
$\log \beta_{H_3B}$	–	–	–	–	17.37
$\log \beta_{CuBH}$	–	–	–	13.46	14.38
$\log \beta_{CuB}$	4.67(9)	4.21	3.44	9.24	10.27
$\log \beta_{CuB_2H}$	–	–	–	21.82	23.96
$\log \beta_{CuB_2H_2}$	–	–	–	21.82	23.96
$\log \beta_{CuB_2}$	8.69(9)	7.55	6.29	16.16	18.49
$\log \beta_{CuB_3}$	–	10.73	8.70	–	–
$\log \beta_{CuB_4}$	–	12.91	10.87	–	–

[a]stz becomes ligand (A) in the mixed ligand complex systems.
[b]see Ref. [21].
[c]see Ref. [19].

Table 2. Stability constants for the Cu(II)–stz(A)–him, bim, hist, and his(B) mixed ligand complex systems at 37°C, $I = 0.15\,\text{mol dm}^{-3}$ ($NaClO_4$).

	Ligand B			
Parameters	him	bim	hist	his
$\log \beta_{CuABH}$	–	–	21.70(9)	22.86(9)
$\log \beta_{CuAB}$	9.87(9)	8.97(8)	14.91(9)	16.27(7)
$\log \beta_{CuAB_2}$	12.98(8)	11.58(8)	–	–
pK^{H}_{CuABH}	–	–	6.79	6.59
$\log K^{CuA}_{CuAB}$	5.20	4.30	10.24	11.60
$\log K^{CuB}_{CuAB}$	5.66	5.53	5.67	6.00
$\log K^{CuBH}_{CuABH}$			8.24	8.48
$\Delta\log K_{CuAB}$	0.99	0.86	1.10	1.27
$\Delta\log K_{CuAB_2}$	0.76	0.62	–	–

Standard deviations are given in parenthesis.

stz in 20 mL aqueous ethanol, and 111/155 mg (5 m mole) of hist/his in 20 mL water; $CuAB_2$ (B = him/bim) complexes were prepared by the addition of 136/238 mg (10 m mole) of him/bim (B) in 20 mL of water. The pH of the reaction mixture was maintained at 5.5 by adding a few drops of 0.002 M NaOH. The contents were kept in a water bath maintained at 60°C with constant stirring. The precipitated solid complexes were filtered, washed with water and ether, further recrystallized using ethanol, and dried in vacuum over fused calcium chloride.

Microanalysis was performed using a Heraeus microanalyzer (Elementar Analysen Systeme, Hanau, Germany). Magnetic susceptibility measurements were carried out using the Gouy balance (Sherwood Scientific Ltd, Cambridge, UK) at 304 K using mercury tetra (thiocyanato) cobaltate(II) as a calibrant. Conductivity measurements were carried out at room temperature on freshly prepared 10^{-3} M DMSO solution using a Systronics 305 conductivity meter (Systronics Ltd, Gujarat, India). Electronic spectra of the complexes were recorded on a Perkin-Elmer 402 spectrometer (PerkinElmer, North America) and IR spectra on a Perkin-Elmer 783 spectrometer

(PerkinElmer, North America) as KBr disks. ESR spectra were recorded in DMSO on a Varian ESR spectrometer (Varian, Palo Alto, California). Powder XRD was performed using a Shimadzu XD-3 diffractometer (Shimadzu Corporation, Japan). SEM measurements were carried out using a JSM-5610 SEM (JEOL, Japan). TGA and DTA were recorded on a Perkin-Elmer 7 series thermal analyzer (PerkinElmer, North America) equipped with Pyres software under a dynamic flow of nitrogen ($10\,L\,min^{-1}$) and heating rate of $10^{\circ}C\,min^{-1}$ from ambient to 700°C. Cyclic voltammetric data of the complexes in MeCN were collected using a BAS C.V. 50 electrochemical analyzer (Artisan Scientific, Champaign, IL, USA). The three-electrode cell contains a reference Ag/AgCl electrode, Pt wire auxiliary electrode, and glassy carbon working electrode. $[Me_4N]ClO_4$ was used as supporting electrolyte and all the potentials are referred to Ag/AgCl.

The *in vitro* growth inhibition of the binary Cu(II)–stz(A) and Cu(II)–stz(A)–him/bim/hist/his (B) complexes were tested against *Sal. typhi*, yeast *Sac. cerevisae* by agar diffusion method [24] and *L. theobrome* and *F. oxysporum* by potato dextrose agar method [24] using agar as nutrient. Ampicillin dissolved in DMF was tested at the same concentration under conditions similar to the complexes. The liquid medium containing bacterial subcultures were autoclaved for 20 min at 121°C at 15 lb pressure before incubation. Bacteria were incubated in nutrient broth at 37°C for 24 h, and fungi and yeast were incubated in Sabouraud dextrose broth at 25°C for 48 h. The bacteria, fungi, and yeast were injected into petri dishes (100 mm × 70 mm) in the amount of $0.01\,cm^3$ and 15 mL of potato dextrose agar was homogenously distributed onto the sterilized petri dishes. All complexes were injected into sterilized antibiotic disks of 6 mm diameter in the amount of 30 mL. The complexes were dissolved in DMF to a final concentration of 2000 ppm and soaked in filter paper. The petri dishes were kept at 4°C for 2 h, then plates inoculated with fungi and yeast were incubated at 25°C for 24 h. The width of the inhibition zone around the disk was measured after 24 h and the activity of each treatment was made in duplicate.

The cleavage of CT DNA was determined by agarose gel electrophoresis by the incubation of samples containing CT DNA, copper complex, and H_2O_2 in tris-HCl/NaCl buffer at 37°C for 2 h. After incubation, the samples were electrophoresed for 2 h at 50 V on 1% agarose gel using tris-acetic acid–EDTA buffer. The gel was then stained using ethidium bromide and photographed under ultraviolet light at 360 nm.

3. Results and discussion

3.1. *Binary complex equilibria*

The ligand stz in its protonated form offers two well-separated buffer regions due to successive deprotonation of NH_3^+ and $-SO_2NH$ moieties. A structurally related compound, 2-benzenesulfonamidopyridene, titrates as a monoprotic acid even in the presence of equimolar amount of acid. The pK_a values are comparable ($pK_a = 9.10$) to that of $-SO_2NH$ moiety [25, 26], suggesting the noninvolvement of hetero N or S in the proton–liquid equilibria of stz. The Cu(II)–stz(A) system showed the presence of CuA and CuA_2 species (table 1). Complex formation of Cu(II) with stz(A) takes place above pH 3, where the ligand predominantly exists in its neutral form. Thus, the NH_2 group

para to $-SO_2NH$ is not involved in coordination. The stz is bidentate [25] through the oxygen of $-SO_2NH$ and the nitrogen of the thiazolidene ring forming a six-membered chelated complex. Complex formation of Cu(II) with stz(A) is accompanied by the change of the color of the solution. The 1 : 2 Cu(II) : stz is violet at pH 5.5 and the λ_{max} of 620 nm is observed. The λ_{max} values do not shift with the change of pH of the solution.

3.2. *Mixed ligand complex equilibria*

The Cu(II)–stz(A)–him/bim(B) systems showed the presence of CuAB and $CuAB_2$ species, while in the Cu(II)–stz(A)–hist/his(B) systems CuABH and CuAB species were detected.

The $\log K^{CuB}_{CuAB}$ values (table 2) compare favorably to each other indicating similar binding of stz with CuAB in all the systems, that is, bidentate in the mixed ligand species as in the binary species. The $\log K^{CuA}_{CuAB}$ values for Cu(II)–stz(A)–bim, him, hist, and his(B) systems (table 2) correspond to monodentate binding of bim and him, bidentate binding of hist, and tridentate binding of his(B) in CuAB. Thus, in CuAB (B = him/bim), three coordination positions would be occupied by the bidentate stz [25] and the monodentate binding of him/bim, the fourth position would be completed by water. In $CuAB_2$, in the him/bim systems, the water in CuAB would be replaced by the second him/bim (figure 2). Again, the $\log \beta_{CuAB}$ value in the hist(B) system is higher than that in $\log \beta_{CuAB_2}$ in the him(B) system (table 2), demonstrating the bidentate binding of hist(B) in CuAB. The $\log \beta_{CuAB}$ value of 16.27 for his is higher than that of hist, 14.91. This suggests that in CuAB his(B) binds tridentate. The $\Delta \log K_{CuAB}$ ($=\log \beta_{CuAB} - \log \beta_{CuA} - \log \beta_{CuB}$) values [27, 28] calculated in all the systems are positive, indicating that B adds on to CuA rather than to the aquated metal ion. The formation of CuAB species is accompanied by a color change in the solution, that is, 1 : 1 : 1 solutions were deep violet at pH 5.5 with λ_{max} values of 670, 655, 680, and 685 nm, respectively, for him, bim, hist, and his systems. The absorbance of the solutions increases with rise in pH, but the λ_{max} value was unaltered.

The CuABH species identified in Cu(II)–stz(A)–hist/his(B) systems are predominantly present in the lower pH regions. The pK^{H}_{CuABH} values (table 2) computed are comparable to each other. Also, $\log K^{CuA}_{CuABH}$ values (table 2) compare favorably with $\log K^{Cu}_{CuBH}$ values (table 1) in the hist and his (B) systems. Protonated binary species has not been detected in the Cu(II)–stz(A) system. These trends clearly demonstrate that the

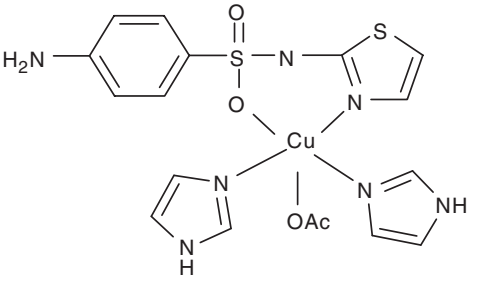

Figure 2. Proposed structure of $CuAB_2$ (B = him).

proton in CuABH is attached with the amino group of hist/his. The $\Delta \log K_{CuABH}$ [27] values in table 2 indicate the marked stabilization of CuABH complexes compared to CuA or CuBH binary complexes.

The species distribution diagrams for all the systems indicate that the mixed ligand complex is more favored over binary analogs. The CuAB species is predominant between pH 5.5 and 6.0, to a maximum of 55% of the total metal ion in 1 : 1 : 1 systems. In the lower pH region CuABH dominates, and on increasing the pH, concentration of CuAB species increases. The representative species distribution diagrams of Cu(II)–stz(A)–him(B) and Cu(II)–stz(A)–his(B) systems are given in figure 3.

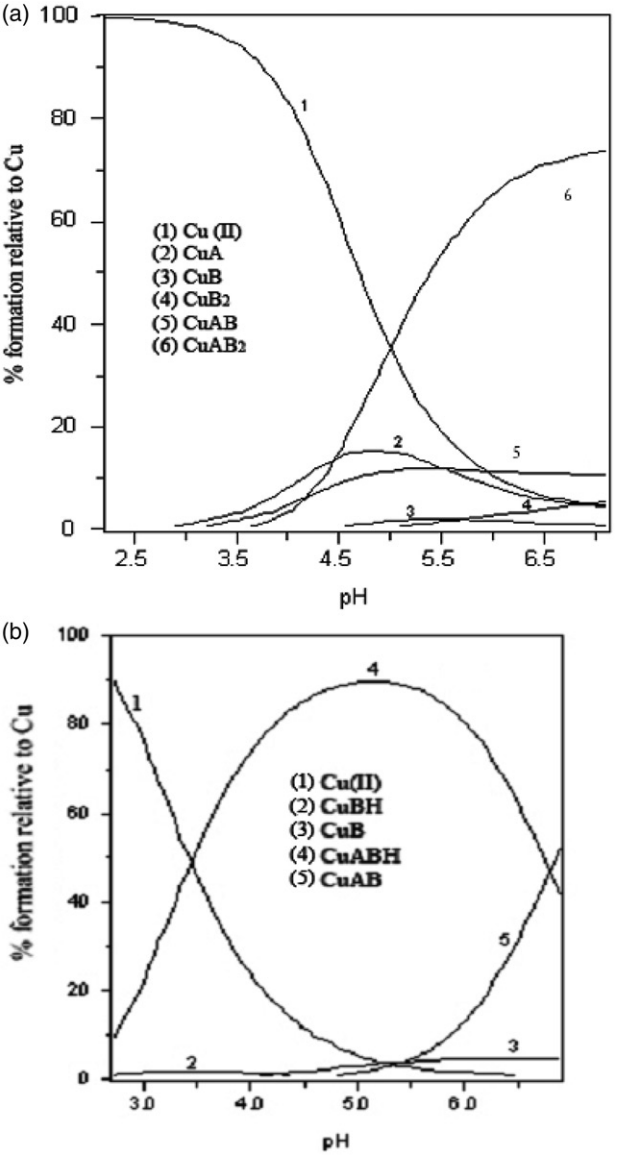

Figure 3. Species distribution diagrams of (a) Cu(II)–stz(A)–him(B) and (b) Cu(II)–stz(A)–his(B).

3.3. *Solid state studies*

All the complexes are insoluble in water and common nonpolar solvents like benzene and ether, but soluble in methanol, ethanol, DMSO, and acetonitrile. The color, melting point, microanalytical data, magnetic susceptibility data, and molar conductance of each complex are given in table 3. Microanalysis data are consistent with CuAB in Cu(II)–stz(A)–hist/his(B) and $CuAB_2$ in Cu(II)–stz(A)–him/bim(B) systems. The molar conductances of the complexes in DMSO for $\approx 10^{-3}$ M solutions at room temperature are low, indicating nonelectrolytes. The μ_{eff} values for Cu(II)–stz(A) and Cu(II)–stz(A)–him/bim/hist/his(B) complexes fall in the range 1.79–1.89 BM, characteristic of d^9 Cu(II) complexes [29].

3.4. *IR spectra of complexes*

The broad band at 3050–3200 cm^{-1} characteristic of free amino group [30] in stz is not altered in the spectra of complexes. This indicates that $-NH_2$ *para* to $-SO_2NH$ is not involved in coordination. Sharp bands at 1360 and 1170 cm^{-1} observed in stz due to the asymmetrical and symmetrical vibration of the sulfonyl group shift to 1323 and 1137 cm^{-1} in complexes, indicating that the oxygen of $-SO_2NH$ bonds to Cu(II). The stz shows absorption bands at 1600, 1020, 927, and 874 cm^{-1}, characteristic of thiazolidene ring, which shift to 1575, 1030, 914, and 893 cm^{-1} in the complexes. This shows that the nitrogen of thiazolidene ring coordinates with the metal. Medium intensity bands at 950, 1085, 1110, 1175, 1285, 1395, and 1495 cm^{-1} due to symmetric stretching vibrations of imidzole [31] in free ligands him/bim/hist/his shift to 960, 1070, 1100, 1190, 1275, 1385, and 1475 cm^{-1} in $CuAB_2$/CuAB complexes, suggesting imidazole binds. The CuAB complex with B = his shows medium intensity bands at 1595 and 1315 cm^{-1} assigned to γ_a(C–O) and γ_s(C–O) of the carboxylate. The difference of $\sim$280 cm^{-1} indicates the monodentate binding of carboxylate of his. A broad band at 3420 cm^{-1} for CuAB (B = his) is attributed to $\gamma_{(O-H)}$ of water coordinated to the complex [29]. $CuAB_2$, B = him and bim, show medium intensity bands, respectively, at 1625 and 1615 cm^{-1} and 1335 and 1330 cm^{-1} assigned to $\gamma_a(CH_3COO^-)$ and $\gamma_s(CH_3COO^-)$. The differences between γ_a and γ_s of $\sim$285 cm^{-1}

Table 3. Elemental analyses, molar conductivities, and melting points of the $CuAB_2$/CuAB complexes.

Compound	Color	Empirical formula	Yield (%)	Found (Calcd) % C	H	N	M	μ_{eff} (BM)	Λ_m (Ω^{-1} cm^2 mol^{-1})	m.p. (°C)
Cu(II)–stz(A)	Pale Purple	$CuC_{22}H_{26}N_6S_4O_8$	65	37.26 (38.06)	3.28 (3.74)	11.90 (12.11)	8.82 (9.15)	1.81	5.78	216
Cu(II)–stz (A)–him(B)	Purple	$CuC_{19}H_{24}N_7S_2O_6$	60	38.82 (39.75)	3.98 (4.18)	16.80 (17.08)	10.84 (11.07)	1.79	8.78	225
Cu(II)–stz (A)–bim(B)	Purple	$CuC_{23}H_{28}N_7S_2O_6$	54	43.32 (44.10)	3.92 (4.47)	14.88 (15.66)	9.95 (10.15)	1.84	10.15	232
Cu(II)–stz (A)–hist(B)	Pale Purple	$CuC_{19}H_{25}N_6S_2O_8$	56	36.60 (37.20)	3.89 (4.30)	14.06 (14.46)	10.96 (11.58)	1.89	12.04	238
Cu(II)–stz (A)–his(B)	Purple	$CuC_{19}H_{25}N_6S_2O_8$	54	38.82 (39.75)	3.91 (4.18)	16.80 (17.08)	10.91 (11.53)	1.86	12.24	244

indicate monodentate acetate [32]. Absorptions at 515–540 cm^{-1} and 410–465 cm^{-1} could be assigned to M–O and M–N bonds [33, 34].

3.5. *Electronic spectra*

The electronic absorption spectra of Cu(II)–stz(A) and Cu(II)–stz(A)–him/bim/hist/his(B) in solution and as solid complexes were recorded at 300 K in ethanol. Absorption assignments and geometry of the binary and mixed ligand complexes are given in table 4. The solid complexes display a broad band at 590–650 nm. In Cu(II)–stz(A)–him/bim(B) absorptions at 596 and 605 nm for $^2B_{1g} \rightarrow {}^2E_g$ favor a square pyramidal geometry [14]. The Cu(II)–stz(A)–hist/his(B) complexes show absorptions at 634 and 646 nm for $^2E_g \rightarrow {}^2T_{2g}$ in distorted octahedral geometry [35, 36].

3.6. *ESR spectra*

X-band ESR spectra of Cu(II)–stz(A)–him and his(B) were recorded in DMSO at 300 and 77 K. The spin Hamiltonian parameters calculated are given in table 5. The spectra of the complexes at 300 K show one intense absorption at high field, isotropic due to the tumbling of molecules. However, four well-resolved peaks with low intensities in the low-field region and one intense peak in the high-field region are observed in the frozen state (Supplementary material). No band corresponding to $m_s = \pm 2$ transition was observed, ruling out the Cu–Cu interaction. The values in table 5 show that $A_\parallel > A_\perp$ and $g_\parallel > g_\perp$, indicating that the unpaired electron lies in the $d_{x^2-y^2}$ orbital [14, 37]. The covalent bonding parameters α^2 (in-plane σ bonding), β^2 (in-plane π bonding),

Table 4. Electronic absorption spectral data of $CuAB_2$/CuAB complexes in solution and solid state at 300 K.

Systems	Species	λ_{max} (nm)	Band assignments	Geometry
Cu(II)–stz(A)	CuA_2	678	$^2E_g \rightarrow {}^2T_{2g}$	Distorted octahedral
Cu(II)–stz(A)–him(B)	$CuAB_2$	596	$^2B_{1g} \rightarrow {}^2E_g$	Square pyramidal
Cu(II)–stz(A)–bim(B)	$CuAB_2$	605	$^2B_{1g} \rightarrow {}^2E_g$	Square pyramidal
Cu(II)–stz(A)–hist(B)	CuAB	634	$^2E_g \rightarrow {}^2T_{2g}$	Distorted octahedral
Cu(II)–stz(A)–his(B)	CuAB	646	$^2E_g \rightarrow {}^2T_{2g}$	Distorted octahedral

Table 5. The spin Hamiltonian parameters of $CuAB_2$/CuAB complexes in DMSO at 77 K.

		Hyperfine constant													
		$A_\parallel$	$A_\perp$	A_{iso}											
Systems	Species	$\times 10^{-4}$ cm^1			$g_\parallel$	$g_\perp$	g_{iso}	α^2	β^2	γ^2	$K_\parallel$	$K_\perp$	$g_\parallel/A_\parallel$	G	
Cu(II)–stz(A)–him(B)	$CuAB_2$	134	84	104	2.28	2.07	2.02	0.75	0.93	0.96	0.69	0.72	170	4.1	
Cu(II)–stz(A)–his(B)	CuAB	135	95	116	2.26	2.06	2.04	0.69	0.86	0.75	0.59	0.52	167	4.5	

and γ^2 (out-of-plane π bonding) were also calculated (table 5). The α^2 of 0.5 indicates covalent bonding, while α^2 equal to 1.0 suggests ionic bonding [38]. The observed α^2 values in table 5 suggest that the complexes have more covalent character. The observed β^2 and γ^2 values indicate in-plane π bonding between metal ion and ligand, also confirmed by orbital reduction factors [39] calculated using the relation $K_{\parallel} = \alpha^2\beta^2$ and $K_{\perp} = \alpha^2\gamma^2$. The trend that $K_{\parallel} < K_{\perp}$ implies a considerable in-plane π bonding and $K_{\parallel} > K_{\perp}$ shows out-of-plane π bonding between metal ion and ligand. The $K_{\parallel}$ and $K_{\perp}$ values in table 5 suggest in-plane π bonding in metal ligand interaction. The linear correlation between $g_{\parallel}$ and $A_{\parallel}$ values have been used to evaluate the degree of distortion in Cu(II) complexes. The g values are related with an exchange interaction coupling constant (G). If the G-value is larger than four, the exchange interaction is negligible because the local tetragonal axes are aligned parallel or slightly misaligned and if the G-value is less than four, the exchange interaction is considerable and the local tetragonal axes are misaligned [40]. The present G-values (table 5) indicate that the local tetragonal axes are aligned parallel or slightly misaligned and consistent with a $d_{x^2-y^2}$ ground state.

3.7. *Powder XRD and SEM analysis*

To obtain further evidence about the structure of the complexes, powder XRD was performed. The d-values of the Cu(II)–stz(A)–him/his(B) complexes, listed in "Supplementary material," match with ASTM data. The Cu(II)–stz(A)–him/his(B) complexes confirm the presence of copper in α-form. ASTM data of stz matches with the d-values of the complexes showing the presence of stz in the complex. Similar observation with the ASTM data d-values of histidine for Cu(II)–stz(A)–his(B) shows the incorporation of histidine in the complex. Strong and broad peaks at $2\theta = 8.5^\circ$ and 10.5° confirm the complex formation and indicate the complex to be microcrystalline [41]. The surface morphology of Cu(II)–stz(A)–him(B)/his(B) complexes by SEM (Supplementary material) shows a disk-like morphology, while Cu(II)–stz(A)–his(B) shows monoclinic-shaped microcrystalline structure. The particle size of the complexes was of a few microns.

3.8. *Thermal analysis*

The TG/DTA shows that Cu(II)–stz(A)–him(B) decomposes in three steps, while Cu(II)–stz(A)–his(B) decomposes in four steps. In Cu(II)–stz(A)–him(B) complex, the first step at 250–400°C with a mass loss of 10.5% and endothermic corresponds to the removal of acetate. The second step at 450–500°C corresponds to the elimination of him with a mass loss of 31%. The final decomposition step at 500–575°C includes the loss of all organic (46%) with the formation of metal oxide (metal content 10.6%). In Cu(II)–stz(A)–his(B), the first and the second steps bring about a mass fraction loss of 6% and 3% within the range of 135–145°C and 175°C–190°C corresponding to the elimination of hydrated and coordinated water [42]. The third step at 300–350°C is due to the loss of his (28%). The final step involves the loss of all ligand (46%) with the formation of metal oxide (10.5%).

3.9. *Electrochemical behavior*

The cyclic voltammograms of Cu(II)–stz(A)–him/his(B) were recorded in MeCN solution at room temperature in the absence of oxygen in the potential range of 1.2–1.6 V. The scan rate used was $100\,mVs^{-1}$. The cyclic voltammetric data (Supplementary material) are similar and show a well-defined quasi-reversible redox peak corresponding to $Cu(II) \rightarrow Cu(III)$ at $Ep_a = 0.92\,V$ and the associated cathodic peak for $Cu(III) \rightarrow Cu(II)$ at $Ep_c = 0.62\,V$ and two irreversible peaks characteristics for $Cu(II) \rightarrow Cu(I)$ ($Ep_c = -0.60\,V$) and $Cu(I) \rightarrow Cu(0)$ ($Ep_c = -1.10\,V$). After an initial scan, if the potential is reversed from $-1.60\,V$, a stripping peak was observed due to the oxidation of deposited metal [43, 44] Cu to Cu(II). The cyclic voltammogram of Cu(II)–stz(A)–his(B) is shown in "Supplementary material".

3.10. *Antimicrobial studies*

The biological activity of Cu(II)–stz(A) and Cu(II)–stz(A)–him/his(B) *in vitro* were tested against *Sal. typhi* and *Sac. cerevisae* by agar diffusion method and *L. theobrome* and *F. oxysporum*. The zone of inhibition against the growth of bacteria, yeast, and fungi for the binary and mixed ligand complexes are given in table 6 (error limit ± 1 mm). The inhibition zones of mixed ligand complexes are higher than binary complex and control [45, 46]. These complexes disturb the respiration of the cell and thus block the synthesis of protein restricting further growth of the organism. Also, the normal cell process may be affected by the formation of hydrogen bonds, through the amino group with the active centers of cell constituents [47].

3.11. *DNA studies*

The oxidative CT DNA cleavage activity of Cu(II)–stz(A) and Cu(II)–stz(A)–him/bim/hist/his(B) were studied using gel electrophoresis (Supplementary material). Cleavage efficiencies of the complexes are compared with control DNA to study the binding ability. Control DNA does not show any significant cleavage of CT DNA. Metal complexes show higher ability to cleave CT DNA than the control and mixed ligand complexes show higher cleavage than binary complex. The presence of smear in the gel diagram indicates radical cleavage [48] by the abstraction of hydrogen from sugar units

Table 6. Biological activity of the $CuAB_2$/CuAB complexes by agar diffusion method [zone formation (mm)].

	Inhibition zone formation (mm) (±1 mm)			
Complex	*Sal. typhi*	*Sac. cerevisae*	*L. theobrome*	*F. oxysporum*
Ampicillin + DMF	55	43	36	39
Cu(II)–stz	61	52	42	48
Cu(II)–stz–him	68	58	51	57
Cu(II)–stz–bim	66	54	46	55
Cu(II)–stz–hist	72	56	48	52
Cu(II)–stz–his	78	61	54	63

of DNA. The metal complexes convert super-coiled DNA into open circular DNA [46], modulated by the bound hydroxyl or peroxo radical generated from H_2O_2.

4. Conclusion

The $CuAB_2$–CuAB mixed ligand complexes were synthesized and characterized using microanalytical and spectroscopic methods. Thermal studies indicate high stability of complexes and powder XRD and SEM analysis show that these complexes are microcrystalline. The antimicrobial activity and CT DNA cleavage ability suggest higher activity for the mixed ligand complexes than binary and control.

Acknowledgements

S. Regupathy wishes to express his gratitude to Dr M.A. Neelakantan, Head, Department of Chemistry, National Engineering College, Kovilpatti, and Dr T.P.D. Rajan, Research Associate, RRL, CSIR, Thiruvananthapuram, for providing the necessary laboratory facilities and constant help.

References

[1] A.J. Lucke, J.D.A. Tyndall, Y. Singh, D.P. Fairlie. *J. Mol. Graphics Model*, **21**, 341 (2003).
[2] K. Vashi, H.B. Naik. *Eur. J. Chem.*, **1**, 272 (2004).
[3] Z.H. Chohan, H. Pervez, A. Rauf, K.M. Khan, C.T. Supuran. *J. Enzyme Inhib. Med. Chem.*, **19**, 417 (2004).
[4] J.R. Anacona, N. Ramos, G. Diaz, E.M. Roque. *J. Coord. Chem.*, **55**, 901 (2002).
[5] M. González-Alvarez, G. Alzuet, J. Borrás, L. del Castillo Agudo, J.M.M. Bernardo. *J. Inorg. Biochem.*, **98**, 189 (2004).
[6] J. Mukta, D. Kumar, R.V. Singh. *Main Group Met. Chem.*, **26**, 99 (2003).
[7] J.J. Plateeuw. *Trop. Med. Int. Health*, **11**, 804 (2006).
[8] M.R. Christiane, C.L.M. Paul, B.M. James. *Clin. Pharm. Kinetics*, **12**, 1247 (2005).
[9] M.J. Anderton, M.M. Manson, R.D. Verschoyle, A. Gester, J.H. Lamp, P.B. Farmer, W.P. Steward, M.L. Williams. *Clin. Cancer Res.*, **10**, 5233 (2004).
[10] V.E. Borisenko, A. Koll, E.E. Kolmakov, A.G. Rjasnyi. *J. Mol. Struct.*, **783**, 101 (2006).
[11] M.S.A. El-Gaby, N.M. Taha, J.A. Micky, M.A.M. Sh. El-Sharief. *Acta Chim. Slov.*, **49**, 159 (2002).
[12] J.R. Anacona, D. Lorono, M. Azocar, R. Atencio. *J. Coord. Chem.*, **62**(6), 951 (2009).
[13] J.R. Anacona, C. Patino. *J. Coord. Chem.*, **62**(4), 613 (2009).
[14] A.A. Azza Abu Hussen, W. Linert. *J. Coord. Chem.*, **62**(9), 1388 (2009).
[15] A. Hossein, M. Mosalla Nejad. *J. Coord. Chem.*, **1**, 11 (2009).
[16] M.S.A. El-Gaby, A.A. Atalla, A.M. Gaber, K.A. Abd Al-Wahab. *Farmaco*, **55**, 596 (2000).
[17] R.E. Staub, C. Feng, B. Dnisko, G.S. Bailey, G.L. Firestone, L.F. Bjeldanes. *Chem. Res. Toxicol.*, **15**, 15 (2002).
[18] H.M. Irving, M.G. Miles, L.D. Pettit. *Anal. Chim. Acta*, **38**, 475 (1967).
[19] M.A. Neelakantan, M.S. Nair. *Iran. J. Chem. Chem. Eng.*, **23**, 97 (2004).
[20] M.S. Nair, M.A. Neelakantan. *J. Indian Chem. Soc.*, **77**, 23 (2000).
[21] M.S. Nair, M. Santappa, P. Natarajan. *J. Chem. Soc., Dalton Trans.*, 1312 (1980).
[22] I.G. Sayce. *Talanta*, **15**, 1397 (1968).
[23] I.G. Sayce, V.S. Sharma. *Talanta*, **19**, 831 (1972).
[24] M.J. Pelczar, E.C.S. Chan, N.R. Kreig. *Microbiology*, 5th Edn, McGraw-Hill, New York (1998) .
[25] G.N. Mukharjee, S. Basu. *J. Indian Chem. Soc.*, **76**, 288 (1999).

[26] A.G. Mohmoud, E. Abdoulkasim, A.H. Amrallah, N.A. Abdulla, O.A. Farghly. *J. Indian Chem. Soc.*, **76**, 480 (1999).
[27] H. Sigel. *Angew. Chem. Int. Ed.*, **14**, 394 (1975).
[28] H. Sigel. In *Metal Ions in Biological Systems*, A. Sigel (Ed.), Vol. 1–37, Marcel Dekker, New York (1971–1997).
[29] B.N. Figgis. *J. Lewis. Inorg. Chem.*, **6**, 37 (1965).
[30] K. Nakamoto. *Infrared and Raman Spectra of Inorganic and Coordination Compounds*, Wiley, New York (1986).
[31] F. Ragot, S. Belin, V.G. Ivanov, D.L. Perry, M. Ortega, T.V. Ignatova, I.G. Kolobov. *Mater. Sci.*, **20**, 3 (2002).
[32] M. Sonmez, M. Sekerci. *Met. Org. Chem.*, **34**(3), 485 (2004).
[33] K.N. Srivatsava, S. Das, R.A. Lal. *Ind. J. Chem.*, **25A**, 85 (1986).
[34] N.S. Biradar, V.L. Roddabasanagoudar, T.M. Aminabhavi. *Polyhedron*, **3**, 575 (1984).
[35] A.B.P. Lever. *Inorganic Electronic Spectroscopy*, Elsevier, New York (1971).
[36] T.M. Dunn. *The Visible and Ultraviolet Spectra of Complex Compounds in Modern Coordination Chemistry*, Interscience, New York (1960).
[37] V.S.X. Anthonisamy, R. Anantharam, R. Murugesan. *Spectrochim. Acta*, **55A**, 135 (1999).
[38] R.S. Drago, M.J. Desmond, B.B. Corden, K.A. Miller. *J. Am. Chem. Soc.*, **105**, 2287 (1983).
[39] D.X. West. *J. Inorg. Nucl. Chem.*, **43**, 3169 (1984).
[40] B.J. Hathaway, A.A.G. Tomlinson. *Coord. Chem. Rev.*, **5**, 1 (1970).
[41] M.G. Abd, E.L. Wahed, S. Abd, E.L. Wanees, M.E.L. Gamel, L. Hameem. *J. Serb. Chem. Soc.*, **69**, 225 (2004).
[42] K.L. El-Baradie, M. Gaber, M. Abusekkina. *Theor. Chim. Acta*, **246**, 175 (1994).
[43] B.E. Roositer, J.F. Hamilton. *Physical Methods of Chemistry-Electrochemical Methods*, Vol. 2, Wiley, New York (1986).
[44] K. Jeyasubramanian, K.A. Samath, S. Tambidurai, R. Murugesan, S.K. Ramalingam. *Transition Met. Chem.*, **20**, 76 (1996).
[45] P.D. Prakash, M.N. Patel. *J. Indian Counc. Chem.*, **20**, 21 (2003).
[46] Y. Anjaneyulu, R.P. Rao. *Synth. React. Inorg. Met-Org. Chem.*, **16**, 257 (1986).
[47] L. Mishra, V.K. Singh. *Ind. J. Chem., Sect. A*, **32**, 446 (1997).
[48] C.X. Zhang, S.J. Lippard. *Curr. Opin. Chem. Biol.*, **7**, 481 (2003).